Structural changes and void generation in low-density amorphous silicon: a computational study

Enrique Guerrero[1, a] and David A. Strubbe[1, b]

[1]*Department of Physics, University of California, Merced, Merced, CA 95343*

(Dated: July 3, 2019)

Abstract

We study the micro-structure of computationally generated amorphous silicon (a-Si) and hydrogenated amorphous silicon (a-Si:H) as a function of density. We use the WWW Monte Carlo method with the Keating potential, using different fixed densities in the generation process. We find a smooth evolution in bond lengths, bond angles, and bond angle deviations $\Delta\theta$ as the density is changed around the equilibrium value of 4.9×10^{22} atoms/cm^3 to higher and lower values. A significant change occurs at densities below 4.3×10^{22} atoms/cm^3 with an onset of void formation, which is associated with a drop in negative pressure, akin to a cavitation process in liquids. We find both small voids (radius $\sim$ 3 Å), as in previous computational studies, and larger ones (up to 7 Å), which compare well with available experimental data. The voids have an influence on atomic structure up to 4 Å beyond the void surface, and are associated with decreasing structural order, measured by $\Delta\theta$. We also observe an increasing medium-range dihedral order with increasing density. The method used to generate structures with voids does not rely on expensive density functional theory molecular dynamics, and allow voids to form naturally by a physical process, without needing any scheme for adding or removing atoms or an a priori idea of void structure. This work provides a set of void structures for further studies of properties such as the Staebler-Wronski effect.

I. INTRODUCTION

Amorphous silicon (*a*-Si) is a cheap and flexible semiconductor used in ultra-reflective mirrors[1], thin-film transistors,[2] and solar cells. A resurgence in interest in the material comes from the designs of hetero-junction with intrinsic thin-layer (HIT) cells, a *c*-Si/*a*-Si tandem solar cell with high efficiency comparable to traditional crystalline silicon (*c*-Si) solar cells.[3] Unfortunately, fielded HIT cells suffer from twice the degradation rate of single-crystal Si cells.[4,5] This increased rate has been attributed to the light-induced Staebler-Wronski degradation[6] of *a*-Si:H which has been attributed to changing Si-H bonds at small voids.[7]

Deposition conditions strongly affect the density and intrinsic stress in *a*-Si:H, and in turn electronic properties such as hole mobilities.[8] Particularly at lower density, voids are found in *a*-Si and *a*-Si:H. Microvoids up to 4 nm have been found using x-ray scattering.[9,10] Voids of this size may be dependent on the production method.[11] Increasing H concentrations can increase the number density of voids[12] and decrease the Young's modulus[13]. Due to the ubiquity of voids, their study is crucial to understanding the macroscopic properties of *a*-Si:H. This work is also motivated by a recent experimental work on voids and variation with density in non-hydrogenated *a*-Si[14,15].

Smaller voids (2−3 Å radius) may be intrinsic: introducing small voids to systems can drop the total energy. Pedersen *et al.*[16] have used this idea to generate realistic, low-energy *a*-Si structures by a grand-canonical Monte Carlo method in which atoms can be removed to find lowest-energy densities and bond topology. Atomic removal methods have previously been studied;[16–19] voids were studied by creating Si mono- or divacancies then passivating dangling bonds with H. The morphology of intrinsic computational voids has been studied by Biswas *et al.*[12,18,20] with meta-dynamics simulations. We complement these studies by exploring voids significantly larger than interstitials (up to 6 Å) at low density instead. Our approach of annealing at constant volume and number of atoms potentially is more closely connected to the physical processes of chemical vapor deposition growth,[8] in which initially deposited Si (and H) atoms on a surface at elevated temperature undergo an annealing process to form the final structure[9]. The melt-quench approach[21] could potentially be used to prepare voids, but voids may be controlled more by bubble formation in the liquid than the properties of the solid network.

Our aim is to generate structures with voids for use in studying the effects on light-

induced degradation[22] and other optoelectronic properties of *a*-Si:H. We use the Wooten-Winer-Weaire[23] method to generate ensembles of *a*-Si and *a*-Si:H at 10% hydrogen content, as is commonly used for electronic devices.[24] We modify the WWW algorithm and observe the formation of voids in the equilibrium structures at a given density, rather than explicitly removing atoms. Typical *a*-Si simulations only consider experimental densities; we instead systematically vary our density and find that the stochastic evolution of our structures favors void formation at low densities. As explored by Pedersen *et al.*,[16] our results imply that voids can lower the total energy, especially at lower densities. Our method is computationally simple and efficient, and does include expensive density functional theory (DFT) or melt-quench molecular dynamics during structure generation. Since we do not remove atoms to create voids, there is no bias on the local topology (e.g. 4 dangling bonds for a monovacancy).

The paper is organized as follows. In Section II, we describe our methods. In section IIA, we describe the modifications to the WWW algorithm used to generate structures as well as overcoming difficulties produced by varying density. Section IIB covers the details of DFT calculations using Quantum Espresso.[25] Section IIC discusses how to characterize voids using Zeo++[26] and how we correlate those voids to structural effects. Section III show results on overall structural changes and then the localized changes near to voids. In Section IV, we conclude.

II. METHODS

A. CHASSM

We use the Computationally Hydrogenated Amorphous Semiconductor Structure Maker (CHASSM)[27] code, which implements the WWW Monte Carlo approach[23]. The ordinary WWW process is described as follows: (1.) Create a periodic *c*-Si structure. (2.) Propose a swap between neighboring bonds and relax the new structure's atomic coordinates. (3.) Compare the proposed structure's energy to the previous structure using the Boltzmann factor $\exp(-\Delta E/k_B T)$ to decide the probability of accepting such a move. (4.) Return to step (2.). CHASSM makes two changes to the initial crystal: we triaxially strain the initial crystal to a target density; and we delete random Si-Si bonds to create a pair of Si-H bonds,[28] up to a desired number of H atoms in the sample. This approach avoids any *a priori* ideas

of where H atoms should go, as involved in schemes of identifying and passivating dangling bonds[12]. Our Keating potential does not have any terms involving the H atoms. In the final structure, an H atom bonded to a given Si atom is considered to be located in a position opposite the Si atoms bonded to it. Structures of a-Si:H from this code, generated in the usual way with a fixed density, have been used to study barriers to bond-switching in the Staebler-Wronski effect[28], strain-induced shifts in Raman peaks,[29] optical absorption,[30] and nanocrystalline sites in a-Si.[31], validated with a variety of properties. Note that given the significant energetic and entropic barriers between different amorphous structures, straining structures to a different density and simply relaxing (as for studying effects of small strain[29]) would not produce as much structural variation as we find here, and would not correspond to the experimental growth to different densities which we are targeting.

We use the Keating classical potential[32] as the energy in the Boltzmann factor. It relies on a predetermined bond table, not a set of distance-based nearest neighbors, to decide which atoms interact. The Keating potential is as follows[32]:

$$U = \frac{3\alpha}{16\delta^2} \sum_{i}^{N_{atoms}} \sum_{j}^{N_{b,i}} \left(\left(|\boldsymbol{r}_{ij}|^2 - \delta^2 \right)^2 + \frac{2\beta}{\alpha} \sum_{k>j}^{N_b,i} \left(\boldsymbol{r}_{ij} \cdot \boldsymbol{r}_{ik} + \frac{\delta^2}{3} \right)^2 \right) \tag{1}$$

where α and β are bond length and angle force constants, δ is the equilibrium Si-Si bond length, $N_{b,i}$ is the number of bonds to atom i (fixed at 4 for a-Si), and $\boldsymbol{r}_{ij}$ is the bond vector from atom i to its jth-bonded atom. We have set α, β, and δ as 2.965 eV/Å^2, 0.845 eV/Å^2, 2.35 Å respectively, to match experimental values for c-Si as used by Barkema and Mousseau.[33] It is interesting to note that the bond-angle term is essentially the tetrahedral order parameter used in system such as amorphous ice.[54]

We allow the structure to evolve using a step-dependent temperature (T) profile to ensure escape of the crystal phase and local minimization in the amorphous regime of the energy landscape. Introducing tensile strain alters the landscape, thus requiring higher initial temperatures to amorphize. The temperature profile consists of three phases. An initial 'randomization' phase of 800 swap attempts/atom at high T (about 0.8 eV) is used to escape the crystal barrier while highly distorting the bonding network. The next 'anneal' phase consists of 100 swap attempts/atom at decreasing T (0.8 to 0.4 eV in $0.002-0.05$ sized intervals); this slow cooling allows improvement of the bonding network while the system traverses small barriers in the rough landscape[34,35] to reach local minima. Finally, we 'quench' (100 swap attempts/atom at $T = 0$) to relax and ensure the system is at a local

minimum.

If the randomization T is too low, the network will not be sufficiently perturbed from a perfect lattice and reverts to a crystal[23] and drop to a low energy as shown in Fig 1. We encountered an opposing problem: if the randomization T too high, the bonding network distorts too far from a physical one to be annealed. Since the Keating potential does not rely on nearest neighbors, atoms may be within coordination shells but have no interaction if they are not "bonded" according to the bond table.[36] Structures with too large a randomization temperature may be artificially over-coordinated: they may have 9+ atoms within the first coordination shell but only four Keating bonds. Structures of this kind will have very high energies shown in Fig 1. To remedy this, we find ideal randomization T empirically: we randomize structures at variable temperatures for 1000 steps for each density, the smallest temperatures that escape the crystal phase are chosen. Ideal temperatures minimize the number of failed structures due re-crystallization or artificial coordination. We find the ideal temperature to be $T = 0.82$ eV$-(\rho - \rho_0)$ 0.18 eV/10^{22} at/cm^3, where $\rho - \rho_0$ is the difference between the density ρ and the relaxed crystal density, $\rho_0 = 5.0{\times}10^{22}$ at/cm^3. At densities below $3.4{\times}10^{22}$ at/cm^3, T required to overcome the initial barrier will always over-distort the bonding network. Densities above 5.8×10^{22} at/cm^3 will always be over-coordinated; we discard structures with any atoms with 5+ atoms within the first coordination shell, since the Keating potential does not describe them well. These facts set the limits of the density range studied in this work. Hydrogenated structures have a larger range of usable T than pure a-Si structures but follow the same ideal T trend, which we attribute to the more flexible bonding network when Si-Si bonds are replaced with Si-H bonds.

The algorithm can also be disrupted by identical bonding: two atoms may be bonded to the same set of four atoms but not to each other. Atoms will inevitably rest on top of each other after relaxation yet feel no mutual interaction. The likelihood of this event increases with the system size and is particularly important to address for structures of 1000+ atoms. We solved this by rejecting moves that would cause two atoms to have the same set of bonds. It could also be remedied by including distance-based repulsive terms to the potential.[36,37]

We use CHASSM to generate ensembles of structures at variable densities of both a-Si (Si_{216}) and a-Si:H ($Si_{216}H_{20}$) from 3.4 to $5.6{\times}10^{22}$ at/cm^3 in intervals of 0.1. 10 structures per density are sampled to be further relaxed using plane-wave DFT. Stresses of ± 1 GPa are common in a-Si:H,[8] and in this work we will go up to around 5 GPa. Cells are fixed as

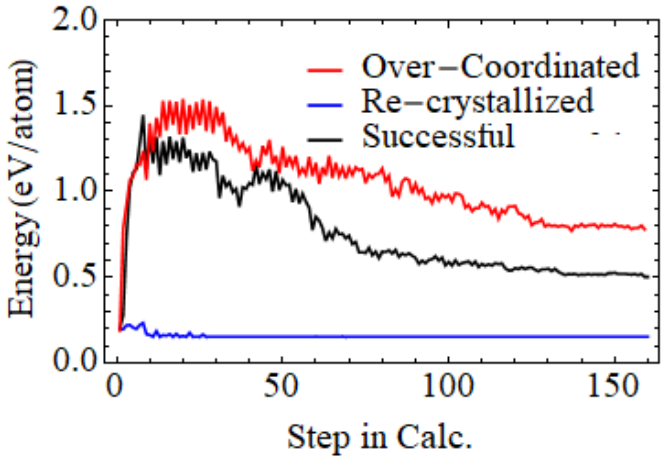

FIG. 1: Keating energy throughout a calculation. The first 8-10 steps are high T randomization. If the structure fails to obtain enough energy to escape the c-Si barrier, it re-crystallizes (blue). If the structure randomizes at too high a T, it does not relax to a reasonable energy (red) or bonding network.

A run producing a desired realistic amorphous structure has an intermediate behavior (black).

simple cubic, with lattice constant ranging from 15.6 Å to 18.5 Å at the highest and lowest densities respectively. Structural parameters of DFT-relaxed structures are calculated and error bars displayed are the standard errors of the population of 10 structures. The structural parameters of the original CHASSM structures in the full data set (bond lengths, bond angles, bond angle deviations) are found to be very similar to the results of DFT relaxation, and are not shown. Pressure results are from a stress calculation in CHASSM implemented in the approach for classical potentials in periodic systems detailed in Ref. 38, using their equations (28) and (29).

B. DFT

We use Quantum Espresso[25] to perform fixed-cell relaxations at the Γ point using the PBE exchange-correlation potential[39] and ultrasoft pseudopotentials (USPP).[40] We set the wavefunction kinetic energy cutoff to 38 Ry and 46 Ry for a-Si and a-Si:H respectively. Charge density cutoffs (requiring special care for USPP) were set to 151 Ry and 221 Ry for a-Si and a-Si:H. WWW structures were relaxed until forces and energies were converged to 10^{-4} Ry/Bohr^2 and 10^{-4} Ry respectively. These values were chosen because lowering

thresholds only affected the atomic positions by less than 10^{-6} Å. Structures at very low and high densities, required smearing to converge the self-consistent cycle, possibly due to unpaired electrons at floating or dangling bonds. For relaxed-density calculations, we perform variable-cell relaxations until the stress tensor elements are below ± 0.01 kbar. *a*-Si structures below 3.6×10^{22} at/cm^3 did not reliably converge scf cycles. After DFT relaxation, we consider atoms within 2.8 Å of each other bonded; bond lengths, angles, and dihedrals are computed from this bonding network.

C. Void Characterization

We delegate our void characterization to Zeo++,[26] an open-source code developed to study the structure of void channels in zeolites. The code's pore-size distribution[41] function samples random "test points" in the material and records the radius of the largest sphere that encapsulate that point without encapsulating any atoms. Note that this method interprets what could be considered a complex-shaped void (as in Ref. 12) as several spherical voids. We have set the atomic radii and probe size to zero, and we have only considered Si atoms for void analysis to be able to directly compare *a*-Si to *a*-Si:H. All structures show a strong peak of interstitial-like voids (Fig 2), a broadened version of the single crystal peak which appears at 2.4 Å. Low-density voids will appear as one or more peaks beyond the interstitial peak. To quantify the total void volume, we ignore the interstitial peak from the distribution. Our void size limit is set by the cell size, but we could study larger voids by increasing the supercell. The void concentration in our low-density calculations is 2 orders of magnitude larger than that found by Biswas around the equilibrum density[12]. To find the atomic densities of the non-void parts of the structure, we set the radii of Si atoms to 2.21 Å, the Van der Waals radius. Renormalized densities are calculated $\rho_{norm} = \rho / N_{atomic}$, where N_{atomic} is the proportion of test points that fall within 2.21 Å of any Si atoms.

We locate large voids by considering test points corresponding to the largest 10% of spheres in a given structure to be that structures "void points" (pictured in Fig 2). We assign a void proximity measure to every atom, r_v, the shortest distance from that atom's center to a void point. We associate this distance with structural parameters to study how far voids' influence extends into the material.

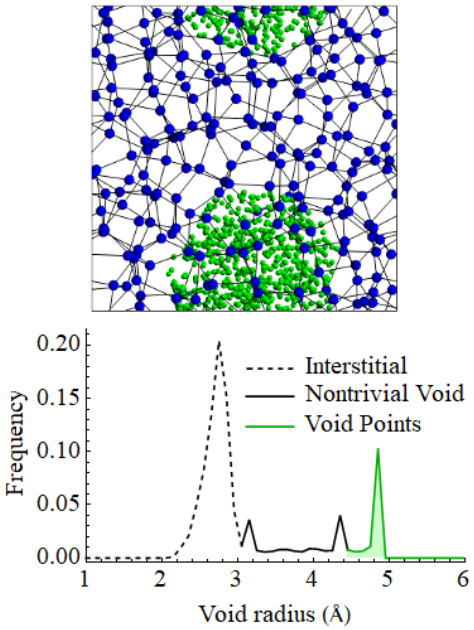

FIG. 2: (top) An example low-density (4.3×10^{22} at/cm^3) a-Si structure with a large void. The green void points fill in the largest voids. (bottom) The pore size histogram of a low-density (4.05×10^{22} at/cm^3) post-DFT structure. Large voids (4.9 Å) and voids of a common size (2.5 Å) appear as strong signals in this histogram. Interstitial voids (dashed) are ignored in void analysis. Area underneath the solid region constitutes the void volume. Only void points belonging to the largest voids (green) are considered for the void proximity (r_v) analysis.

III. RESULTS AND DISCUSSION

We can probe the differences between pre- and post-DFT bond topologies to assess the validity of CHASSM structures. Any atoms whose local bonding has been readjusted (whether by a broken or new bond) is counted as a bond correction. Away from relaxed densities, these events are more common, at worst 3% compared to the 0% near relaxed densities. Atomic positions are corrected by DFT on average by 0.04 Å. We take these as evidence that DFT preserves the topology created by the Keating potential reasonably well, except at the most extreme densities we have studied.

We benchmark the density, elastic properties, and structural parameters at the relaxed density in Table III. The densities of both c-Si and a-Si are underestimated by PBE by 0.1×10^{22} at/cm^3. The relaxed c-Si CHASSM density (by choice of the Keating parameters α, β, and δ) matches experiment, but a-Si is incorrectly denser than c-Si, as noted in the

	CHASSM			**CHASSM +DFT**			**Exp't**		
	c-Si	a-Si	a-Si:H	c-Si	a-Si	a-Si:H	c-Si	a-Si	a-Si:H
ρ_0	5.01	5.12	5.07	4.87	4.78	4.67	5.01[42]	4.9[43]	4.9[44]
Y	162	180	166	153	138	129	165[42]	140[43]	134[44]
B	97	77	64	82	59	60	98[42]	59[45]	59[45]
$< r_0 >$	2.35	2.33	2.34	2.37	2.36	2.38	2.35[42]	2.38[46]	2.38[46]
$< \theta >$	109.5	109.3	109.3	109.5	109.2	109.1	109.5	108.4[46]	108.4[46]
$\Delta\theta$	0	9.6	9.9	0	10.3	11.0	0	8-11[46,47]	8-11[46,47]

TABLE I: Relaxed density parameters of CHASSM, CHASSM+DFT, and experimental c-Si, a-Si, and a-Si:H. Density values are in 10^{22} at/cm^3, Young's moduli (Y) and bulk moduli (B) are in GPa, mean bond lengths ($< r >$) are in Å, and mean bond angles ($< \theta >$) and angle deviations ($\Delta\theta$) are in degrees.

original WWW work.[23] This does not affect results for a fixed density though. Elastic constants are described well by CHASSM only for c-Si near relaxed densities (Fig. 4), due to the lack of any dependence beyond harmonic in the Keating potential, but the DFT elastic constants agree well with experiment. Structural parameters agree well with experiment, and we find similar levels of agreement for a-Si and a-Si:H.

Our calculated pair distributions $g(r)$ are shown in Fig. 3. We find they have little dependence on density, and are very similar for a-Si and a-Si:H. A 2.2 Å peak in the H-H pair distribution function is consistent with SiH_2 bonding networks found in divacancies created with molecular dynamics by Chakraborty and Drabold.[17] This peak is a sign that H atoms preferentially cluster near the interior of voids.

Pressures (trace of the stress tensor) calculated using the Keating potential are significantly lower than those obtained from DFT, but they have a similar trend with a constant offset in Fig 4. Pressures vary linearly with density above 4.5×10^{22} at/cm^3. A sudden drop in absolute pressure occurs at the critical density between 4.3 and 4.5×10^{22} at/cm^3, showing stress relief. These densities are consistent with the onset of voids in Fig. 5. This behavior shows the same physical mechanism as cavitation and bubble formation at low pressures in liquids.[48,49] We thus conclude that voids have been created to relieve the global pressure,

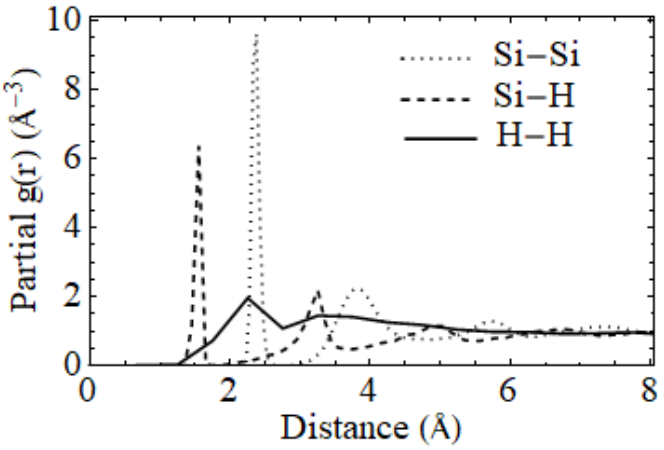

FIG. 3: Averaged partial pair distribution functions, $g(r)$, for a-Si:H at all densities. $g(r)$ for a-Si is identical to the Si-Si distribution in a-Si:H. Decreasing density increases the height of the H-H 2.2 Å peak, but has little effect on the other curves.

when the bonding network has stretched too much and cannot sustain further pressure. The pressure stabilizes to a constant value at the lowest densities for all data sets. This stabilization may be related to the saturated drop of elastic modulus in the studies by Jiang[13]. At low densities, small voids coalesce into one large void or even large channels. This could be related to the observation in liquids that at low enough densities, spherical cavitation evolves to cylindrical cavitation.[48] At any rate, once voids approach the size of our supercell, they are likely to meet their periodic neighbors and form connected channels.

This picture of cavitation is reinforced by examination of the bond lengths and angles (Fig. 6), which have a transition around the critical density 4.3×10^{22} at/cm^3. Bond lengths in a-Si increase as density is decreased, but then decrease again back to the relaxed value after stress relief with void formation. The small magnitude of bond length changes seem consistent with the results of Jacks and Molina-Ruiz *et al.*,[14,15] from electron-energy loss spectroscopy (EELS). Overall, a-Si:H structures react more smoothly to strain because of the degrees of freedom discussed in section II A. The increase in $\Delta\theta$ at low density, the typical measurement of amorphous order as inferred from the TO peak width in a Raman spectrum,[53] is also consistent with Jacks and Molina-Ruiz *et al.*,[14,15], although we see a larger increase, perhaps due to finite-size effects of our supercell or limitations in the experimental extraction of $\Delta\theta$ and density in the films. We find that $\Delta\theta$ increases at high densities also. The average bond angle decreases away from the relaxed density too, more dramatically for

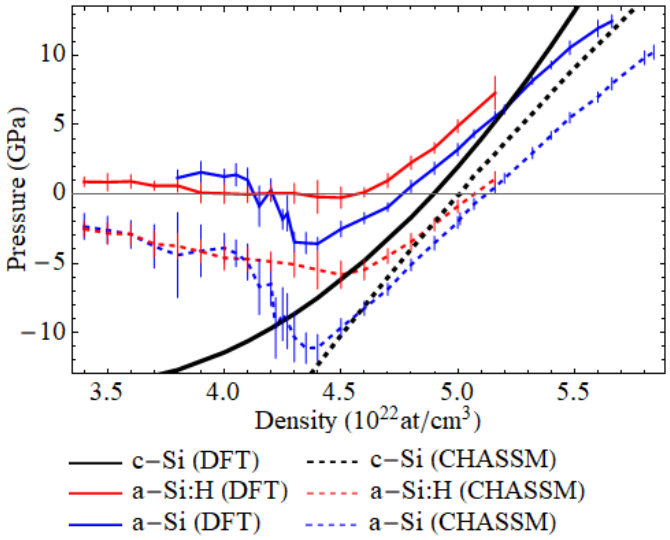

FIG. 4: CHASSM (solid) and CHASSM + DFT (dashed) calculated pressures vs. densities. As density is decreased in a-Si and a-Si:H, negative pressure is induced, but then relieved near the void onset density of 4.3–4.5$\times 10^{22}$ at/cm^3, like the cavitation process of bubble formation. CHASSM pressures are systematically too low compared to DFT, but have the correct trend. a-Si has a more abrupt transition than a-Si:H.

a-Si, which we will interpret in terms of effects near voids. The energies in CHASSM and DFT show increases away from the relaxed density, of course, but also a clear bump at the critical density for a-Si; no obvious feature occurs for a-Si:H. A constant trend of $< r >$ at low densities is consistent with the stabilized renormalized density in Fig. 5. These plots combined imply that Si-Si bonds have stopped stretching and begin to relax as a result of cavitation. Flattening of this atomic network density at low global densities is consistent with Rutherford backscattering spectroscopy and atomic force microscopy data.[14,15]

Dihedral distributions show an unexpected density-induced variation. It is often considered that there is a uniform distribution of dihedrals in a-Si, inferred from the third nearest-neighbor peak in $g(r)$ as measured by X-ray diffraction.[50] However, our results show instead sinusoidal variation, with distinct peaks at 60° and 180° similar to what has been found in other computational studies[16,51] and inferred by Laaziri.[52] For comparison, c-Si has 2/3 of the dihedrals as 60° and 1/3 as 180°. To describe the density dependence, we restrict ourselves to Si atoms only and fit the dihedral distributions to the form $A\cos(2\pi/120°)+D$. D is density-invariant, but A, which we term the dihedral amplitude, is a measure of the

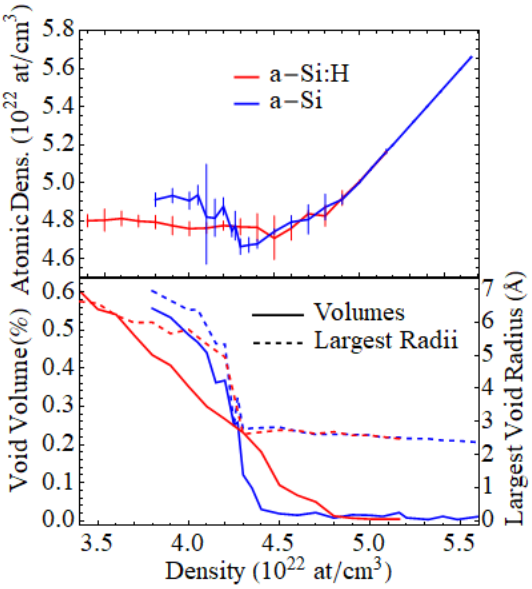

FIG. 5: Renormalized atomic densities (top) indicate the density of the non-void regions, showing that void formation allows the rest of the sample to retain a constant density. (bottom) The encapsulating sphere method directly confirms that voids start forming at 4.3–4.5 $\times$ 10^{22} at/cm^3. Above the critical density, largest void radii are of about the size of the interstitial and total void volume is nearly 0% of the total volume.

strength of dihedral order. Increasing the density increases the magnitude of A (Fig 7), indicating a stronger medium range order at high densities. Lowest density structures seem to show a complete flattening such that $A \to 0$. Below 4.3 $\times$ 10^{22} at/cm^3, the relationship reverses and angles at 0° and 120° are more likely to be found than 60° or 180°. Curiously, the lowest density a-Si structures with strong 0° peaks are found to contain hexagonal bi-layer sheets (like a graphene bilayer with AA stacking). We presume that these structures are unphysical artefacts of the Keating potential, and indeed the change of structure with DFT relaxation is increasingly large around these densities. Hexagonal bilayer sheets are compatible with large free surfaces while tetrahedrally coordinated structures necessarily suffer large deformations to their bond angles near a void. In a-Si:H, A does not go above 0 and we have not found evidence of hexagonal sheet structures.

In low-density structures with large voids, structural deformations are associated with void proximity, r_v. To isolate local structural parameters from, we group atoms based on their r_v and collect bond lengths and angles associated with those atoms. $\Delta\theta$, $< \theta >$, and

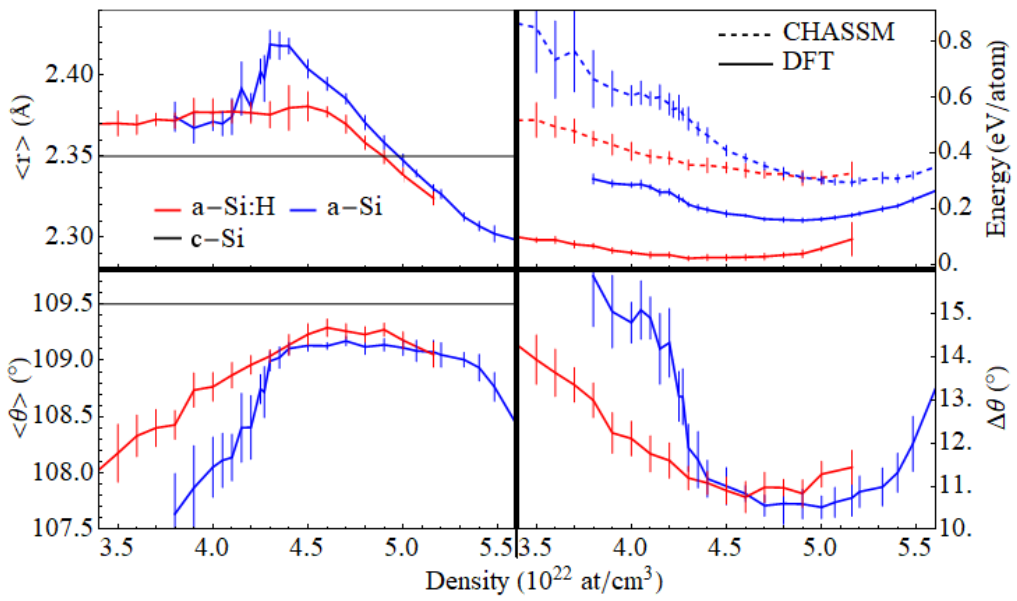

FIG. 6: Response of structural parameters to density variation. Bond lengths and angles change trends around 4.3×10^{22} at/cm^3, the density of void onset shown in Fig. 5. Relaxed c-Si has a CHASSM energy of 0 eV and $\Delta\theta = 0$. a-Si DFT energies are relative to c-Si, a-Si:H energies are relative to the lowest a-Si:H energy in our data set.

$< r >$ are now computed on those sub-populations. Accurate description is limited by half the cell size minus the void diameter, to a distance of about 7 Å away from a void surface. In a given low-density structure, the increased bond angle deviation resides entirely around the surface of voids shown in Fig 8. Away from voids, the deviation returns to relaxed-like values of 10°. We have pictured the motif for increase in local bond angles in Fig 8. These results show conclusively that the structural changes below the void formation critical density are driven by the voids.

Fig 3 provides evidence that H atoms tend to cluster in a-Si:H. We use a similar r_v analysis to find that H atoms are highly concentrated near voids, especially at low densities. This is significant since we did not explicitly place H atoms at the void surfaces, as in some previous work, but the H atoms naturally ended up there from the Monte Carlo process and annealing. This result is consistent with previous studies.[17,58]

Finally, ring analysis (calculated using King's method[55] with the open-source code R.I.N.G.S.[56]) are consistent with previous works.[57] There is little density-dependence in the ring statistics of a-Si:H. An increase in a-Si 6-membered rings at the lowest densities is

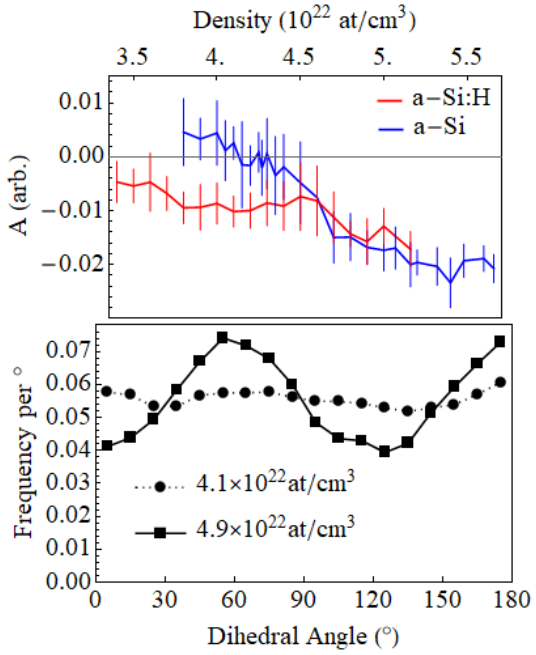

FIG. 7: (top) The relationship between density and the dihedral amplitude, A, in low and high density a-Si structures. A is a direct measure of the dihedral order, it increases as the density increases. (bottom) Dihedral distributions for a low (4.1×10^{22} at/cm^3) and relaxed (4.9×10^{22} at/cm^3). Dihedral order vanishes at the lowest densities.

present—consistent with the observed hexagonal sheets.

IV. CONCLUSION

Using a pure WWW method with different fixed densities, we are able to generate realistic a-Si and a-Si:H structures with voids, that can be used to study degradation or phenomena. The method is simple and scales well with system size,[33] and requires no atomic addition or removal, or any *a priori* idea of the targeted structures. The voids arise as equilibrium structures at densities below a critical density. We find in a-Si:H that H atoms tend to be concentrated near voids. We verified the validity of the WWW and Keating potential description across a range of densities near the relaxed one, except for the most extreme densities studied.

Structural analysis of a-Si and a-Si:H at low density indicate less tetrahedral bond angle distributions and nonlinear bond lengths stretching. a-Si:H responds more smoothly to

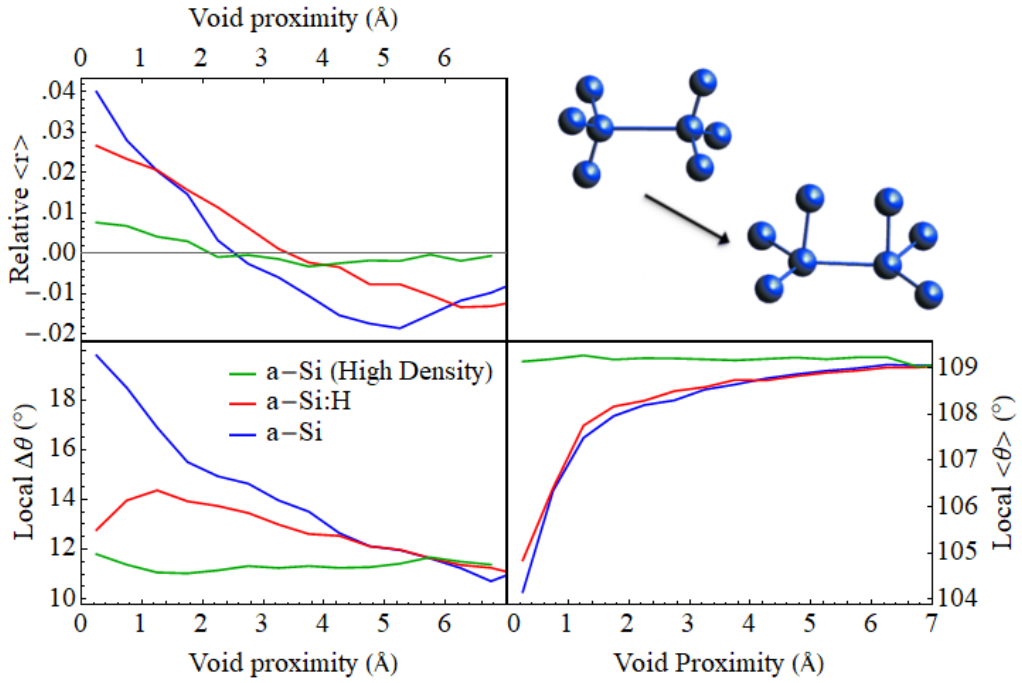

FIG. 8: Locally resolved structural response of low density structures as a function of void proximity. a-Si and a-Si:H lines are structures below 4.3×10^{22} at/cm^3. High density structures (green) are plotted to contrast, since the largest voids in these structures are not distinguishable from interstitials there is little correlation between structural deformation and void proximity. $< r >$ are calculated with respect to average bond lengths for each given density. The results are consistent with a local rearrangement of bonds to accommodate a void as shown in the top-right sketch.

strain than a-Si due to a less constrained network. The increase in negative pressure and then reduction below the cirtical density indicates the bonding network undergoes a bubble-like cavitation process—the formation of large voids to relieve internal stresses. By resolving structures at an atomic level, we conclude that the structural changes at low density reside near void surfaces.

V. ACKNOWLEDGMENTS

We acknowledge useful discussions with Gergely Zimányi, Frances Hellman, Manel Molina-Ruiz, and Hilary Jacks. We acknowledge support from UC Merced start-up funds and from the Merced nAnomaterials Center for Energy and Sensing (MACES), a NASA-funded research and education center, under award NNX15AQ01. This work used com-

putational resources from the Multi-Environment Computer for Exploration and Discovery (MERCED) cluster at UC Merced, funded by National Science Foundation Grant No. ACI-1429783, and the National Energy Research Scientific Computing Center (NERSC), a U.S. Department of Energy Office of Science User Facility operated under Contract No. DE-AC02-05CH11231.

---

[a] Electronic address: eguerrero23@ucmerced.edu

[b] Electronic address: dstrubbe@ucmerced.edu

[1] J. Steinlechner, I. W. Martin, A. S. Bell, J. Hough, M. Fletcher, P. G. Murray, R. Robie, S. Rowan, and R. Schnabel, Phys. Rev. Lett. **120**, 263602 (2018), URL https://link.aps.org/doi/10.1103/PhysRevLett.120.263602.

[2] A. Nathan, A. Kumar, K. Sakariya, P. Servati, S. Sambandan, and D. Striakhilev, IEEE Journal of Solid-State Circuits **39**, 1477 (2004), ISSN 0018-9200.

[3] K. A. Bush, A. F. Palmstrom, Z. J. Yu, M. Boccard, R. Cheacharoen, J. P. Mailoa, D. P. McMeekin, R. L. Z. Hoye, C. D. Bailie, T. Leijtens, et al., Nature Energy **2**, 17009 EP (2017), article, URL https://doi.org/10.1038/nenergy.2017.9.

[4] D. C. Jordan, C. Deline, S. Johnston, S. R. Rummel, B. Sekulic, P. Hacke, S. R. Kurtz, K. O. Davis, E. J. Schneller, X. Sun, et al., IEEE Journal of Photovoltaics **8**, 177 (2018), ISSN 2156-3381.

[5] T. Ishii and A. Masuda, Prog. Photovolt: Res. Appl. **25**, 953 (2017).

[6] D. L. Staebler and C. R. Wronski, Appl. Phys. Lett. **31**, 292 (1977).

[7] M. Fehr, A. Schnegg, B. Rech, O. Astakhov, F. Finger, R. Bittl, C. Teutloff, and K. Lips, Phys. Rev. Lett. **112**, 066403 (2014), URL https://link.aps.org/doi/10.1103/PhysRevLett.112.066403.

[8] E. Johlin, C. B. Simmons, T. Buonassisi, and J. C. Grossman, Phys. Rev. B **90**, 104103 (2014).

[9] A. H. M. Smets, W. M. M. Kessels, and M. C. M. van de Sanden, Applied Physics Letters **82**, 1547 (2003), https://doi.org/10.1063/1.1559657, URL https://doi.org/10.1063/1.1559657.

[10] S. C. Moss and J. F. Graczyk, Phys. Rev. Lett. **23**, 1167 (1969), URL https://link.aps.org/doi/10.1103/PhysRevLett.23.1167.

[11] M. Vanecek, J. Holoubek, and A. Shah, Applied Physics Letters **59**, 2237 (1991),

https://doi.org/10.1063/1.106081, URL https://doi.org/10.1063/1.106081.

[12] P. Biswas, D. Paudel, R. Atta-Fynn, D. A. Drabold, and S. R. Elliott, Phys. Rev. Applied **7**, 024013 (2017), URL https://link.aps.org/doi/10.1103/PhysRevApplied.7.024013.

[13] X. Jiang, B. Goranchev, K. Schmidt, P. Grnberg, and K. Reichelt, Journal of Applied Physics **67**, 6772 (1990), https://doi.org/10.1063/1.345064, URL https://doi.org/10.1063/1.345064.

[14] H. C. Jacks, Ph.D. thesis, University of California, Berkeley (2019).

[15] M. Molina-Ruiz, H. C. Jacks, D. Castells-Graells, A. Ceballos, J. Maldonis, P. Voyles, M. H. Weber, and F. Hellman., in preparation.

[16] A. Pedersen, L. Pizzagalli, and H. Jónsson, New Journal of Physics **19**, 063018 (2017), URL https://doi.org/10.1088%2F1367-2630%2Faa732e.

[17] S. Chakraborty and D. A. Drabold, Phys. Rev. B **79**, 115214 (2009), URL https://link.aps.org/doi/10.1103/PhysRevB.79.115214.

[18] P. Biswas, R. Atta-Fynn, S. Chakraborty, and D. A. Drabold, Journal of Physics: Condensed Matter **19**, 455202 (2007), URL https://doi.org/10.1088%2F0953-8984%2F19%2F45%2F455202.

[19] S. M. Nakhmanson and D. A. Drabold, Phys. Rev. B **61**, 5376 (2000), URL https://link.aps.org/doi/10.1103/PhysRevB.61.5376.

[20] P. Biswas and S. R. Elliott, Journal of Physics: Condensed Matter **27**, 435201 (2015), URL https://doi.org/10.1088%2F0953-8984%2F27%2F43%2F435201.

[21] M. D. Kluge, J. R. Ray, and A. Rahman, Phys. Rev. B **36**, 4234 (1987), URL https://link.aps.org/doi/10.1103/PhysRevB.36.4234.

[22] G. T. Zimanyi, C. Hansen, and D. A. Strubbe, in *Proceedings of the 46th IEEE Photovoltaic Specialists Conference* (2019).

[23] F. Wooten, K. Winer, and D. Weaire, Phys. Rev. Lett. **54**, 1392 (1985).

[24] R. A. Street, *Hydrogenated Amorphous Silicon*, Cambridge Solid State Science Series (Cambridge University Press, 1991).

[25] P. Giannozzi, S. Baroni, N. Bonini, M. Calandra, R. Car, C. Cavazzoni, D. Ceresoli, G. L. Chiarotti, M. Cococcioni, I. Dabo, et al., J. Phys.: Condens. Matter **21**, 395502 (2009).

[26] T. F. Willems, C. H. Rycroft, M. Kazi, J. C. Meza, and M. Haranczyk, Microporous and Mesoporous Materials **149**, 134 (2012), ISSN 1387-1811, URL http://www.sciencedirect.

com/science/article/pii/S1387181111003738.

[27] D. A. Strubbe, L. K. Wagner, E. C. Johlin, E. Guerrero, and J. C. Grossman, *Computational Hydrogenated Amorphous Semiconductor Structure Maker (CHASSM)* (2019), in preparation.

[28] L. K. Wagner and J. C. Grossman, Phys. Rev. Lett. **101**, 265501 (2008).

[29] D. A. Strubbe, E. C. Johlin, T. R. Kirkpatrick, T. Buonassisi, and J. C. Grossman, Phys. Rev. B **92**, 241202 (2015), URL https://link.aps.org/doi/10.1103/PhysRevB.92.241202.

[30] R. Raghunathan, E. Johlin, and J. C. Grossman, Nano Letters **14**, 4943 (2014), ISSN 1530-6984, URL https://doi.org/10.1021/nl501020q.

[31] T. Mueller, E. Johlin, and J. C. Grossman, Phys. Rev. B **89**, 115202 (2014), URL https://link.aps.org/doi/10.1103/PhysRevB.89.115202.

[32] P. N. Keating, Phys. Rev. **145**, 637 (1966), URL https://link.aps.org/doi/10.1103/PhysRev.145.637.

[33] G. T. Barkema and N. Mousseau, Phys. Rev. B **62**, 4985 (2000), URL https://link.aps.org/doi/10.1103/PhysRevB.62.4985.

[34] P. Charbonneau, J. Kurchan, G. Parisi, P. Urbani, and F. Zamponi, Nature Communications **5**, 3725 EP (2014), article, URL https://doi.org/10.1038/ncomms4725.

[35] F. H. Stillinger and T. A. Weber, Science **225**, 983 (1984), ISSN 0036-8075, https://science.sciencemag.org/content/225/4666/983.full.pdf, URL https://science.sciencemag.org/content/225/4666/983.

[36] S. von Alfthan, A. Kuronen, and K. Kaski, Phys. Rev. B **68**, 073203 (2003), URL https://link.aps.org/doi/10.1103/PhysRevB.68.073203.

[37] F. H. Stillinger and T. A. Weber, Phys. Rev. B **31**, 5262 (1985), URL https://link.aps.org/doi/10.1103/PhysRevB.31.5262.

[38] A. P. Thompson, S. J. Plimpton, and W. Mattson, The Journal of Chemical Physics **131**, 154107 (2009), https://doi.org/10.1063/1.3245303, URL https://doi.org/10.1063/1.3245303.

[39] J. P. Perdew, K. Burke, and M. Ernzerhof, Phys. Rev. Lett. **77**, 3865 (1996), URL https://link.aps.org/doi/10.1103/PhysRevLett.77.3865.

[40] D. Vanderbilt, Phys. Rev. B **41**, 7892 (1990), URL https://link.aps.org/doi/10.1103/PhysRevB.41.7892.

[41] M. Pinheiro, R. L. Martin, C. H. Rycroft, A. Jones, E. Iglesia, and M. Haranczyk, Journal of Molecular Graphics and Modelling **44**, 208 (2013), ISSN 1093-3263, URL http://www.

sciencedirect.com/science/article/pii/S109332631300096X.

[42] M. A. Hopcroft, W. D. Nix, and T. W. Kenny, Journal of Microelectromechanical Systems **19**, 229 (2010), ISSN 1057-7157.

[43] A. Witvrouw and F. Spaepen, Journal of Applied Physics **74**, 7154 (1993), https://doi.org/10.1063/1.355031, URL https://doi.org/10.1063/1.355031.

[44] R. Kuschnereit, H. Fath, A. Kolomenskii, M. Szabadi, and P. Hess, Appl. Phys. A **61**, 269 (1995).

[45] K. Tanaka, Solid State Communications **60**, 295 (1986), ISSN 0038-1098, URL http://www.sciencedirect.com/science/article/pii/0038109886904692.

[46] J. Fortner and J. S. Lannin, Phys. Rev. B **39**, 5527 (1989), URL https://link.aps.org/doi/10.1103/PhysRevB.39.5527.

[47] P. Roura, J. Farjas, and P. Roca i Cabarrocas, Journal of Applied Physics **104**, 073521 (2008), https://aip.scitation.org/doi/pdf/10.1063/1.2990767, URL https://aip.scitation.org/doi/abs/10.1063/1.2990767.

[48] P. Wang, W. Gao, J. Wilkerson, K. M. Liechti, and R. Huang, Extreme Mechanics Letters **11**, 59 (2017), ISSN 2352-4316, URL http://www.sciencedirect.com/science/article/pii/S2352431616302036.

[49] M. Blander and J. Katz, AIChE Journal **21**, 833 (1979).

[50] W. Schlke, Philosophical Magazine B **43**, 451 (1981), https://doi.org/10.1080/01418638108222109, URL https://doi.org/10.1080/01418638108222109.

[51] M. Park, I.-H. Lee, and Y.-S. Kim, Journal of Applied Physics **116**, 043514 (2014), https://doi.org/10.1063/1.4891500, URL https://doi.org/10.1063/1.4891500.

[52] K. Laaziri, S. Kycia, S. Roorda, M. Chicoine, J. L. Robertson, J. Wang, and S. C. Moss, Phys. Rev. B **60**, 13520 (1999), URL https://link.aps.org/doi/10.1103/PhysRevB.60.13520.

[53] D. Beeman, R. Tsu, and M. F. Thorpe, Phys. Rev. B **32**, 874 (1985), URL https://link.aps.org/doi/10.1103/PhysRevB.32.874.

[54] E. Dubou-Dijon and D. Laage, The Journal of Physical Chemistry B **119**, 8406 (2015), pMID: 26054933, https://doi.org/10.1021/acs.jpcb.5b02936, URL https://doi.org/10.1021/acs.jpcb.5b02936.

[55] S. V. King, Nature **213**, 1112 (1967), ISSN 1476-4687, URL https://doi.org/10.1038/

2131112a0.

[56] S. L. Roux and P. Jund, Computational Materials Science **49**, 70 (2010), ISSN 0927-0256, URL http://www.sciencedirect.com/science/article/pii/S0927025610002363.

[57] V. L. Deringer, N. Bernstein, A. P. Bartók, M. J. Cliffe, R. N. Kerber, L. E. Marbella, C. P. Grey, S. R. Elliott, and G. Csányi, The Journal of Physical Chemistry Letters **9**, 2879 (2018), URL https://doi.org/10.1021/acs.jpclett.8b00902.

[58] A. C. Wright, A. C. Hannon, R. N. Sinclair, T. M. Brunier, C. A. Guy, R. J. Stewart, M. B. Strobel, and F. Jansen, Journal of Physics: Condensed Matter **19**, 415109 (2007), URL https://doi.org/10.1088%2F0953-8984%2F19%2F41%2F415109.